Article type: Full paper

Schottky Barrier-Controlled Black Phosphorus/Perovskite Phototransistors with Ultrahigh Sensitivity and Fast Response

*Xuming Zou, Yuanzhe Li, Guanqi Tang, Peng You, and Feng Yan**

Dr. X. Zou, Dr. Y. Li, Dr. G. Tang, Dr. P. You, Prof. F. Yan
Department of Applied Physics, The Hong Kong Polytechnic University, Hong Kong, China
Dr. X. Zou
Key Laboratory for Micro/Nano Optoelectronic Devices of Ministry of Education & Hunan Provincial Key Laboratory of Low-Dimensional Structural Physics and Devices, School of Physics and Electronics, Hunan University, Changsha 410082, China
* Corresponding email: F Yan, Email: apafyan@polyu.edu.hk, Tel:(852) 2766 4054, Fax:(852) 2333 7629

Key words: phototransistor; black Phosphorus; perovskite; ultrahigh sensitivity; fast response

Phototransistors have been recognized as highly sensitive photodetectors owing to their high gain induced by a photogating effect. However, the response speed of a typical phototransistor is rather slow due to the long lifetime of trapped carriers in the channel. Here, we report a novel Schottky barrier-controlled phototransistor that shows ultrahigh sensitivity as well as a fast response speed. The device is based on a channel of few-layer black phosphorous modified with a $MAPbI_{3-x}Cl_x$ perovskite layer, whose channel current is limited by the Schottky barrier at the source electrode. The photo-response speed of the device can be tuned by changing the drain voltage, which is attributed to a field-assisted detrapping process of electrons in the perovskite layer close to the Schottky barrier. Under optimal conditions, the device exhibits a high responsivity of 10^6–10^8 A/W, an ultrahigh specific detectivity up to 9×10^{13} Jones and a response time

of ~10 ms.

1. Introduction

Photodetectors have demonstrated important applications in various fields, including industrial and environmental monitoring,[1] threat detection,[2] medical imaging,[3] free-space communication,[4] remote control,[5] and so forth.[6,7] It is highly desirable to have photodetectors with high detectivity (D^*), fast response, broadband spectrum coverage, room-temperature operation and low cost. Two-dimensional (2D) layered materials, such as graphene, transitional metal dichalcogenides (TMDCs)[8-11] and black phosphorous (BP), have been extensively investigated for the applications of photodetectors due to their unique two dimensional nature, high carrier mobilities and tunable band structure. However, existing photodetectors based on 2D materials normally exhibit low responsivity (R) (10^{-4}-10^{-1} A/W) due to the weak light absorption of the few atomic layers,[8-11] making it difficult to achieve high sensitivity in photodetection. To solve this problem, hybrid phototransistors with 2D materials modified with other photosensitive materials, such as quantum dots (QDs),[12-16] organic dyes,[17] carbon nanotubes[18,19] and perovskite materials,[20-24] have been investigated in recent years. Due to a strong photogating effect induced by trapped carriers in the photosensitive layers, the devices can show ultrahigh gain and responsivity. For example, Konstantatos et al. reported hybrid graphene/PbS quantum dots (QDs) phototransistors that exhibited high responsivity up to ~10^7 A/W.[12,13] Lee et al. reported a graphene/$MAPbI_3$ perovskite phototransistor that showed a high responsivity

of ~10^6 A/W.[20] Recently, our group developed an ultrasensitive phototransistor by inserting an electron blocking layer between graphene and $MAPbI_3$, resulting in a responsivity of 1.4×10^9 A/W.[21] Besides, Kang et al. demonstrate a $MoS_2/MAPbI_3$ phototransistor with a responsivity of 2.1×10^4 A/W.[22] Most recently, $WS_2/MAPbI_3$ and $WeSe_2/MAPbI_3$ heterostructures are also exploited for highly sensitive phototransistors.[23,24] However, the reported high responsivities and gains rely on long lifetimes of carriers (on the scale of seconds to minutes) in the photosensitive layers of the phototransistors, which inevitably causes slow response speeds of the devices. Until now, how to realize phototransistors with both ultrahigh responsivity and fast response speed is still a grand challenge yet to be tackled.

Here, we present a novel Schottky barrier-controlled phototransistor that has the channel current limited by the Schottky barrier at the source electrode. The device is based on a few-layer BP crystal channel modified with $MAPbI_{3-x}Cl_x$ perovskite layer on the top. Due to a high electric field near the Schottky barrier, photo-generated carriers (electrons) in the perovskite layer can be quickly extracted by the source electrode, leading to a fast response speed of the device. The Schottky barrier-controlled phototransistor exhibits a high responsivity up to 10^8 A/W, a short response time down to ~10 ms and an ultrahigh specific detectivity up to 9×10^{13} Jones, which are much better than the performance of the previously reported phototransistors.

2. Results and Discussion

Photogating effect refers to the modulation of the channel current in a phototransistor

by light illumination. In a traditional phototransistor, one type photocarriers are trapped in the channel for a long period and another type carriers can transport in the channel with a high mobility, leading to a photo gain (G) given by:[12]

$$G = \tau_{lifetime}/\tau_{transit} \quad (1)$$

where $\tau_{transit}$ is the transit time for the transporting carriers in the channel and $\tau_{lifetime}$ is the lifetime of the trapped photocarriers. Meanwhile, the response time of the phototransistor is at the same order of the lifetime of the trapped photocarriers. To achieve a high gain of the phototransistor, $\tau_{lifetime}$ should be much longer than $\tau_{transit}$, which however will lead to a slow response speed of the device.

To overcome the drawback of conventional phototransistors, we design a Schottky barrier-controlled phototransistor based on BP and $MAPbI_{3-x}Cl_x$ perovskite, which has the channel current limited by the Schottky barrier at the source electrode instead of the conductance of the channel. As shown in Figure 1a, a Schottky barrier is introduced in the phototransistor between the source electrode and the perovskite-modified BP channel by using a low work function metal (Al or Cr) as the source electrode. The current across the Schottky barrier is related to the barrier height (ψ_B) and given by:[25]

$$I_{ds}=A^*T^2 \exp\left(-q\psi_B/k_BT\right)\left(\exp(qV/k_BT)-1\right) \quad (2)$$

where A^* is effective Richardson constant, ψ_B is the barrier height, V is the bias voltage applied on the junction, k_B is the Boltzmann constant, q is the elementary charge and T is the absolute temperature. At ideal conditions, the barrier height ψ_B is given by:

$$\psi_B = E_v - \phi_m \quad (3)$$

where E_v is the energy level of the valence band and ϕ_m is the work function of the metal electrode. Meanwhile, the barrier height ψ_B can be modulated by electric field E due to the Schottky effect.

The schematic of the energy diagram of BP/$MAPbI_{3-x}Cl_x$ perovskite hybrid structure with Al electrode is shown in Supporting Information Figure S1. The Fermi level offset at the BP/perovskite heterojunction will induce band bending and accelerate the selective hole transfer from perovskite to BP. The working principle of the Schottky barrier-controlled phototransistor is demonstrated in Figure 1. Under light illumination, electron and hole pairs will be generated in the perovskite layer. Due to the band banding at the BP/perovskite heterojunction, holes will diffuse to BP channel and electrons will accumulate in the perovskite layer. The accumulated electrons will induce an additional electric field near the Schottky barrier to decrease the barrier height as shown in Figure 1b,e. The electrons in the perovskite layer can have relatively long carrier lifetimes when they are trapped by localized states especially boundary states. This is the reason why traditional phototransistors based on perovskite and 2D materials normally show long response times.[20-22, 24] In the Schottky barrier-controlled phototransistor, the lifetime of electrons in the perovskite layer near the source electrode (see Figure 1b) can be shortened by introducing an electric field E close to the source electrode due to a field-assisted detrapping process, called Frenkel-Poole (FP) emission.[25] Interestingly, a high electric field near the source electrode can be easily introduced by applying a source-drain voltage V_{ds} because the channel resistance of the transistor is much lower than the Schottky barrier resistance. Therefore, the

response time of the phototransistor can be tuned by changing V_{ds}, which is confirmed by our following experiments.

In our experiments, ultrathin BP crystal flakes (~5-8 nm thick) are produced by repeated splitting of bulk BP crystals using a mechanical cleavage method, and subsequently transferred to silicon substrates covered with 290 nm-thick thermal oxide. We chose 5-8 nm thick few-layer BP flakes because BP with this thickness is less susceptible to surface oxidation in ambient conditions in comparison with thinner samples and can maintain a reasonably high mobility as well as large on/off ratio in transistor operation.[26-29] Then, Cr or Al source electrodes and Au (60 nm) drain electrodes are patterned on top of the BP flakes by e-beam lithography and thermal evaporation. Because Cr (ϕ_m = 4.5 eV) and Al (ϕ_m = 4.3 eV) have lower work functions than Au (ϕ_m = 5.1 eV),[30] Schottky barriers can be formed at the source electrodes while Ohmic contact can be obtained at drain electrodes.

Next, $MAPbI_{3-x}Cl_x$ perovskite films are deposited with the conventional one-step spin-coating method.[31,32] Figure 2a shows optical images of a typical BP transistor before and after the coating of $MAPbI_{3-x}Cl_x$ perovskite. Figure 2b shows the SEM image of the as-prepared $MAPbI_{3-x}Cl_x$ film on silicon substrate, which exhibits compact polycrystalline texture with full surface coverage and an average grain size of ~300 nm. As shown in the inset of Figure 2b, the thickness of the $MAPbI_{3-x}Cl_x$ film is ~220 nm. Figure 2c shows the X-Ray diffraction (XRD) spectrum of the perovskite thin film. The strong diffraction peaks at 14.09°, 28.43°, 43.23°, and 58.90° can be assigned to (110), (220), (330), and (440) lattice planes, indicating the tetragonal structure of the $MAPbI_{3-}$

$_xCl_x$ perovskite. Meanwhile, there is no PbI_2 or $PbCl_2$ diffraction peaks observed in the XRD spectrum, so the reaction of $PbCl_2$ with methylammonium iodide is complete and a pure $MAPbI_{3-x}Cl_x$ phase is formed.

Figure 2d shows the absorption spectra of an as-fabricated $MAPbI_{3-x}Cl_x$ film. Strong and broadband absorption in UV−visible range with a sharp absorption edge located at ~800 nm can be observed. Figure 2e shows the Raman spectra of a pristine BP flake and a BP/perovskite heterostructure. The typical Raman peaks of few-layer BP are observed at 362, 439, and 467 cm^{-1}, which are assignable to the A^1_g, B^2_g and A^2_g phonon modes,[33] respectively. After the perovskite coating, we cannot observe the variation of peak positions, indicating that the deposition of $MAPbI_{3-x}Cl_x$ film via one-step method does not induce a detectable change in the BP flake.

The photoluminescent (PL) spectra of the samples measured with the excitation of 532 nm laser are presented in Figure 2f. Both the perovskite–only and hybrid BP/perovskite films exhibit a peak of ~1.6 eV, which is consistent with the bandgap of $MAPbI_{3-x}Cl_x$. More importantly, compared with perovskite–only film, significant PL quenching exceeding 90% is observed in the BP/perovskite heterostructure under the same experimental conditions. This is the direct evidence for the transfer or the separation of photogenerated electrons and holes at the BP/perovskite interface. In the phototransistor, the perovskite film with a thickness of ~220 nm can harvest sufficient light on the detection area and lead to pronounced hole inject into the BP layer.

Three types of BP transistors defined as Au-Au, Cr-Au and Al-Au devices with Au, Cr and Al source electrodes, respectively, were characterized before the deposition of

perovskite layers. Figure 3a-c show the transfer characteristics (I_{ds} vs V_{gs}) of the three devices. All devices show an ambipolar behaviour due to the small bandgap of the BP channel ($E_g \approx 0.4$ eV). The Schottky contact in the device using a Cr or Al source electrode plays an important role on the device performance. In the p-channel side of the transfer curve ($V_{gs} < 30$ V), the channel current is dramatically decreased when the polarity of V_{ds} is changed from positive to negative (+2 V changed to -2 V) because negative V_{ds} induces hole injection from the source electrode to the channel, which is limited by the Schottky barrier. Since the work function of Al is lower than that of Cr, the Schottky barrier for holes at the Al/BP junction is higher than that at the Cr/BP junction, leading to a lower injection current of the former. If we check the hole current under positive V_{ds}, the channel currents are not mainly limited by the Schottky barrier and thus the magnitudes of the currents are very similar in all three devices.

To further study the contact effect in the transistors, the output characteristics (I_{ds} vs V_{ds}) of the three devices are measured, as shown in Figure 3d-f. Apparently, the device with Au-Au electrodes shows symmetric Ohmic contact behaviour while a current-rectifying characteristic is observed when using Cr-Au or Al-Au electrodes. The rectification ratio ($I_{Vds=+2V}/I_{Vds=-2V}$) is also dependent on the gate voltage as shown in the inset of the figures and Supporting Information Figure S2. The rectification ratio is increased from ~20 for Cr-Au contacts to ~80 for Al-Au contacts, indicating a higher Schottky barrier height at Al source electrode. From a detailed temperature-dependent study that considers both thermionic emission and thermally assisted tunneling over the Schottky barrier,[34-38] the barrier height is determined to be ~0.15 eV for the Cr contact

and ~0.23 eV for the Al contact (see Supporting Information Figure S3). The extracted barrier height are lower than the ideal values (~0.6 eV for the BP/Cr contact and ~0.8 eV for the BP/Al contact),[27, 30, 39] which can be attributed to trap states at the metal/BP interface.

Figure 4a shows the transfer curves (I_{ds} *vs* V_{gs}; V_{ds} = -2 V) of a Schottky barrier-controlled phototransistor with Al-Au electrodes before and after the coating of $MAPbI_{3-x}Cl_x$ perovskite layer. The pristine BP device without a perovskite layer exhibits an ambipolar behaviour with an on/off ratio exceeding 10^4. After the coating of $MAPbI_{3-x}Cl_x$, the transfer curve shifts parallel to a higher gate voltage, suggesting a p-type doping effect in the BP channel induced by the perovskite layer.[15,16, 20] Under light illumination at a wavelength of 598 nm and an intensity of 45.9 μW/cm^2, the transfer curve shifts to more positive voltages because of the injection of holes into the channel, which is similar to previously reported photogating devices.[12-24] To identify the optimum gate voltage, we extract the responsivity (R) and the light-to-dark current ratio (I_{light}/I_{dark}) from the transfer curves and present the data in Figure 4b. The maximum responsivity of 4×10^6 A/W can be obtained at the gate voltage of about -30 V.

We find that the device responsivity is dependent on light intensity. As shown in Figure 4c**,** the responsivity increases with the decrease of the light intensity, following a relationship of the form $R \sim E_e^{\beta-1}$, which is due to the increase of electron lifetime with the decrease of hole density at the BP/perovskite interface.[12, 40] When the light intensity is decreased to 0.4 μW/cm^2, the responsivity is increased to 1.1×10^7 A/W

under the operational voltages of V_{gs}=30V and V_{ds}=-2V. The maximum responsivity observed at the gate voltage of V_{gs}=-30V is 1.9×10^{8}A/W. This result is three orders of magnitude higher than those of TMDCs/$MAPbI_{3-x}Cl_x$ hybrid photodetectors reported before.[22-24] In addition, we also performed the same measurements under illumination at the wavelength of 370 or 895 nm. Although the light absorption of the perovskite is relatively low at a wavelength beyond 800 nm, the responsivity of the device can be as high as 5.2×10^{5} A/W at 895 nm under a gate bias of 30V. The photoresponse in the NIR region beyond the absorption edge of the $MAPbI_{3-x}Cl_x$ perovskite can be attributed to the excitation of carriers from the valence band to the traps states within the perovskite bandgap, similar to the extrinsic photoconductors based on normal semiconductors.[41]

Figure 4d,e show the transient behaviour of a phototransistor under a light source switched on and off for many times with increasing light intensities and a constant intensity, respectively. The stable photocurrents at different states demonstrate a good reproducibility of the device. As shown in the inset of Figure 4e, the rise time and decay time (τ_{rise} and τ_{decay}) are measured to be 8 and 17 ms, respectively, which are several orders of magnitude lower than the values for previously reported photogating devices.[12,13, 20-22, 24] The rise (decay) time here is defined as the period for the photocurrent to rise (decay) from 10% to 90% (90% to 10%) of the final value. Figure 4f shows the normalized responsivity of the device in the broad wavelength region from UV to NIR (350 nm to 1200 nm) at the same light intensity. Therefore, the device can be used as a broadband photodetector with an ultrahigh sensitivity.

Besides responsivity, specific detectivity is another key parameter to characterize

the capability of detecting the weakest light signal and given by:[25, 42-45]

$$D^* = \frac{(SB)^{1/2}}{NEP} \tag{4}$$

$$NEP = \frac{\overline{i_n^2}^{1/2}}{R} \tag{5}$$

where B is bandwidth, NEP is the noise equivalent power, $\overline{i_n^2}^{1/2}$ is the root mean square value of the noise current. The noise level per unit bandwidth (1 Hz) of the phototransistor is measured to be ~30 pA/Hz$^{1/2}$ under the operational voltages of V_{gs}=30V and V_{ds}=-2V. (see Supporting Information Figure S4). Using the R values of 5.5×10^6, 1.1×10^7 and 5.2×10^5 A/W at the wavelength of 370, 598 and 895 nm, the corresponding D^* values are calculated to be 4.6×10^{13}, 9.2×10^{13}, and 4.3×10^{12} Jones (cmHz$^{1/2}$/W), respectively, which are superior to those of the traditional silicon photodetectors.[25]

Next, the influence of the Schottky-barrier height on the transient property of the phototransistors is investigated. Figure 5a-c show the detailed rise/decay processes of the channel currents (V_{ds} = -2 V and V_{gs} = 0 V) when the devices were illuminated with a light intensity of 0.4 μW/cm^2. The rise (decay) time for the devices with Au-Au, Cr-Au and Al-Au electrodes are 2.5 s (19.1 s), 0.9 s (1.9 s) and 40 ms (60 ms), respectively. It is notable that the device with Au-Au ohmic contacts has the longest response time, which is similar to the response speed of perovskite-based phototransistors reported before.[20-22, 24] In contrast, the devices with Schottky barriers in the channel exhibit much faster photo responses.

For our photogating transistors, both the rise time and decay time are limited by

the life times of electrons trapped in the perovskite layers on BP channels. As shown in Figure 1b, the trapping/detrapping process of electrons in the perovskite layer can be activated by the electric field close to the source electrode, which is dependent on the applied drain voltage V_{ds}. For a device with a higher Schottky barrier, the potential drop on the Schottky barrier is higher due to the higher resistance of the junction. Consequently, a higher electric field close to the source electrode can be induced, which will extract electrons in the perovskite layer with a higher speed. Therefore, the carrier lifetime of electrons in the perovskite layer decreases with the increase of barrier height. This relationship explains why a phototransistor with a higher Schottky barrier can show a faster response speed.

Figure 5d shows the influence of drain voltage V_{ds} on the response time of the phototransistor with Al-Au electrodes. The same measurements for Au-Au and Cr-Au contacts are shown in Supporting Information Figure S5. The extracted rise/decay times are presented in Figure 5e,f. We can find that the rise/decay time decreases with the increase of $|V_{ds}|$ and can be modulated for about 1 order of magnitude, which can be attributed to the increased electric field E close to the source electrodes. This effect can also be observed in the Au-Au device without a Schottky barrier although the shortest response lifetime is longer than one second. In this case, the electric field is uniformly distributed in the channel and electrons in the whole perovskite layer can be moved by the drain voltage with a low speed. The unique characteristic of the voltage-tunable response speed of the phototransistor will be very useful in practical applications and can be utilized in the design of circuits to achieve a desirable detection speed.

Figure 5f presents the responsivity of the devices as a function of V_{ds}. It is reasonable to find the increase of responsivity with the increase of V_{ds}. Notably, the device with Au-Au ohmic contact exhibits the highest responsivity (2.0×10^9 A/W) at a low light intensity of 0.4 μW/cm^2, which is comparable to those of previously reported perovskite photodetectors and other state-of-art photodetectors. According to equation (1), the gain of the phototransistor is equal to $\tau_{lifetime}/\tau_{transit}$. Here, the lifetime of holes in BP is related to the trapping time of electrons in $MAPbI_{3-x}Cl_x$ perovskite, which could be presented by the response time (~2.5 s) of the device. So the gain of the device G is estimated to be about 10^{10}. Therefore, it is reasonable to find the high responsivity of the BP/$MAPbI_{3-x}Cl_x$ phototransistor due to the photogating effect. In comparison, the Schottky barrier-controlled phototransistor with Al-Au electrodes shows a lower responsively (1.9×10^8 A/W) but a much faster response speed, making it more useful in practical applications. To demonstrate the high performance achieved by our novel Schottky barrier-controlled phototransistors in comparison with the previously reported devices, we summarize the key figures-of-merit in Table S1.

To better understand the device physics, we performed 2-dimensional device simulation using a commercial software. As shown in Figure 6a, the phototransistor with the BP/perovskite channel was simulated under light illumination. Notably, the experimental data for the transfer curves induced by the coating of perovskite layer and the photogating effect can be fitted very well by the software (see Supporting Information Figure S6). The effect of the Schottky barrier height on the transfer curve of the BP transistor can also be fitted (see Supporting Information Figure S7). Hence,

the local electric field close to the Schottky barrier of the source electrode under different V_{ds} can be extracted, as shown in Figure 6b,c. The FP current density (J) has the following relationship with the electric field (E):

$$J = AE \ \ exp(-\frac{q(\varphi_b - \sqrt{qE/\pi\varepsilon_0\varepsilon_r})}{k_B T}) \quad (6)$$

where A is the preexponential factor, ε_r is the dynamic dielectric constant of perovskite, φ_b is the FP trap energy (i.e., the energy level of the trap with respect to the conduction energy level of the perovskite). Assuming the decay time is inversely proportional to the FP current, we can obtain the relationship:

$$ln\left(\frac{1}{\tau_{decay}E}\right) = R\sqrt{E} + S \quad (7)$$

where R and S are constants. Notably, the linear relationship of $ln(1/\tau_{decay}E)$ vs $\sqrt{E}$ for the Al-Au phototransistor is confirmed in Figure 6d, which is a proof for the validity of FP emission model in describing the detrapping process with reasonable physical parameters.

3. Conclusion

In conclusion, we design and fabricate a new type of Schottky barrier-controlled phototransistor based on BP and $MAPbI_{3-x}Cl_x$ perovskite. Being different from traditional phototransistors, the device can demonstrate high responsivity as well as fast response time due to a field-assisted detrapping process of photo-generated carriers in the channel. The phototransistor shows an ultrahigh responsivity up to 10^8 A/W and a high specific detectivity up to 9×10^{13} Jones in a broad wavelength region from UV to NIR. Meanwhile, the response time of the device is optimized to be ~10 ms, which is

several orders of magnitude faster than those achieved in high-gain phototransistors reported before. This unique design opens a window for realizing new-generation high-performance photodetectors compatible with traditional microelectronics.

4. Experimental Section

Device fabrication: Few-layer BP flakes are mechanically exfoliated from bulk BP crystals and transferred to the pre-cleaned highly doped p-type silicon substrates with a thermally grown 290 nm thick SiO_2 layer. Then the substrates are spin-coated with PMMA, and the EBL (JEOL 6510 with NPGS) is employed to define the source and drain pattern. The metal electrodes are deposited by thermal evaporation and lift-off processes. Subsequently, the fabricated devices are heated at 250 °C for 2 h in a nitrogen-filled glove box to drive off water molecules. MAI and $PbCl_2$ (99.5 wt %) are dissolved in anhydrous N,N-dimethylformamide (DMF) (99.8 wt %) at a 3:1 molar ratio, and stirred at 50 °C for 12 h inside a nitrogen-filled glovebox to produce a mixed halide perovskite precursor solution. In order to fabricate the BP/$MAPbI_{3-x}Cl_x$ phototransistor, the precursor solution is spin-coated on the silicon substrates at 4000 rpm for 1 min and annealed at 100 °C for 60 min to form a $MAPbI_{3-x}Cl_x$ perovskite film with a thickness of ~220 nm.

Material and Device Characterization: The surface and cross-sectional morphologies of the perovskite film are characterized by scanning electron microscopy (SEM) using FEI Nova 450 Nano. X-ray diffraction (XRD) measurement is performed using a Rigaku SmartLab X-ray Diffractometer operated at room temperature. The

UV−vis absorption spectra are recorded on a Shimadzu UV-2550 UV−vis spectrometer. Raman spectra are recorded by using a Horiba's LabRam HR high resolution spectrometer equipped with a multichannel CCD detection system in backscattering configuration. The incident laser light can be focused on the sample within a spot of 1-2 μm in diameter. PL are performed using a 532 nm excitation laser at room temperature. Electrical and optoelectrical measurements are performed by using a semiconductor parameter analyzer (Keithley 4200A-SCS) under light illumination with different intensities in a glovebox. The light sources are light emitting diodes (LEDs) with wavelengths of 370, 598, and 895 nm, respectively. Spectral response tests were performed using a standard quantum efficiency measurement system equipped with a xenon lamp (Oriel 66902, 300W, Newport Corporation, Irvine, CA, USA), a monochromator (Newport 66902, Irvine, CA, USA), a Si detector (Oriel 76175-71580, Newport Corporation), and a dual-channel power meter (Newport 2931-C).

Acknowledgements

This work is financially supported by the Research Grants Council (RGC) of Hong Kong, China (Project No. PolyU 152087/17E), the Hong Kong Polytechnic University (Project No. 1-YW0Y), NSFC grant (Nos. 61704051) and Hunan Province Natural Science Foundation (2017JJ3033).

Received: ((will be filled in by the editorial staff))

Revised: ((will be filled in by the editorial staff))

Published online: ((will be filled in by the editorial staff))

References:

[1] U. Willer, M. Saraji, A. Khorsandi, P. Geiser, W. Schade, *Opt. Lasers Eng.* **2006**, *44*, 699.

[2] D. S. Moore, *Rev. Sci. Instrum.* **2004**, *75*, 2499.

[3] A. Zecchina, C. O. Areán, *Chem. Soc. Rev.* **1996**, *25*, 187.

[4] R. Soref, *Nat. Photonics* **2010***, 4*, 495.

[5] R.-H. Yuang, J.-I. Chyi, W. Lin, Y.-K. Tu, *Opt. Quantum Electron.* **1996***, 28*, 1327.

[6] X. Gong, M. H. Tong, Y. J. Xia, W. Z. Cai, J. S. Moon, Y. Cao, G. Yu, C.-L. Shieh, B. Nilsson, A. J. Heeger, *Science* **2009**, *325*, 1665.

[7] G. Konstantatos, E. H. Sargent, *Nat. Nanotechnol.* **2010**, *5*, 391.

[8] T. Mueller, F. N. Xia, P. Avouris, *Nat. Photonics* **2010**, *4*, 297.

[9] F. Xia, T. Mueller, Y.-m. Lin, A. Valdes-Garcia, P. Avouris, *Nat. Nanotechnol.* **2009**, *4*, 839.

[10] N. Perea‐López, A. L. Elías, A. Berkdemir, A. Castro‐Beltran, H. R. Gutiérrez, S. Feng, R. Lv, T. Hayashi, F. López‐Urías, S. Ghosh, *Adv. Funct. Mater.* **2013**, *23*, 5511.

[11] W. Choi, M. Y. Cho, A. Konar, J. H. Lee, G. B. Cha, S. C. Hong, S. Kim, J. Kim, D. Jena, J. Joo, *Adv. Mater.* **2012**, *24*, 5832.

[12] G. Konstantatos, M. Badioli, L. Gaudreau, J. Osmond, M. Bernechea, F. P. G. De Arquer, F. Gatti, F. H. Koppens, F. H. *Nat. Nanotechnol.* **2012**, *7*, 363.

[13] [a)] Z. H. Sun, Z. K. Liu, J. H. Li, G. a. Tai, S. P. Lau, F. Yan, *Adv. Mater.* **2012**, *24*, 5878. [b)] J. H. Li, L. Niu, Z. J. Zheng and F. Yan, *Adv. Mater.* **2014**, 26, 5239. [c)] Z. K. Liu, J. H. Li, and F. Yan, *Adv. Mater.* **2013**, 25, 4296. [d)] Z. K. Liu, J. H. Li, Z. H. Sun, G. Tai, S. P. Lau and F. Yan, *ACS Nano* **2012**, 6, 810.

[14] D. Zhang, L. Gan, Y. Cao, Q. Wang, L. Qi, X. Guo, *Adv. Mater.* **2012**, *24*, 2715.

[15] N. Huo, S. Gupta, G. Konstantatos, *Adv. Mater.* **2017***, 29*, 1606576.

[16] D. Kufer, I. Nikitskiy, T. Lasanta, G. Navickaite, F. H. L. Koppens, G. Konstantatos, *Adv. Mater.* **2015**, *27*, 176.

[17] Y. S. Gim, Y. Lee, S. Kim, S. Hao, M. S. Kang, W. J. Yoo, H. Kim, C. Wolverton, J. H. Cho, *Adv. Funct. Mater.* **2016**, *26*, 6593.

[18] Y. Liu, F. Wang, X. Wang, X. Wang, E. Flahaut, X. Liu, Y. Li, X. Wang, Y. Xu, Y. Shi, R. Zhang, *Nat. Commun.* **2015**, *6*, 7.

[19] Y. Liu, Y. Liu, S. Qin, Y. Xu, R. Zhang, F. Wang, *Nano Res.* **2017**, *10*, 1880.

[20] Y. Lee, J. Kwon, E. Hwang, C.-H. Ra, W. J. Yoo, J.-H. Ahn, J. H. Park, J. H. Cho, *Adv. Mater.* **2015**, *27*, 41.

[21] C. Xie, P. You, Z. Liu, L. Li, F. Yan, *Light: Sci. Appl.* **2017**, *6*, e17023.

[22] D.-H. Kang, S. R. Pae, J. Shim, G. Yoo, J. Jeon, J. W. Leem, J. S. Yu, S. Lee, B. Shin, J.-H. Park, *Adv. Mater.* **2016**, *28*, 7799.

[23] C. Ma, Y. Shi, W. Hu, M.-H. Chiu, Z. Liu, A. Bera, F. Li, H. Wang, L.-J. Li, T. Wu, *Adv. Mater.* **2016**, *28*, 3683.

[24] J. P. Lu, A. Carvalho, H. W. Liu, S. X. Lim, A. H. Castro Neto, C. H. Sow, *Angew. Chem.* **2016**, *128*, 12124.

[25] S. M. Sze, K. K. Ng, *Physics of semiconductor devices*. John wiley & sons: **2006**.

[26] F. N. Xia, H. Wang, Y. C. Jia, *Nat. Commun.* **2014**, *5*, 4458.

[27] L. Li, Y. Yu, G. J. Ye, Q. Ge, X. Ou, H. Wu, D. Feng, X. H. Chen, Y. Zhang, *Nat. Nanotechnol.* **2014**, *9*, 372.

[28] X. Chen, C. Chen, A. Levi, L. Houben, B. Deng, S. Yuan, C. Ma, K. Watanabe, T. Taniguchi, D. Naveh, X. Du, F. Xia, *ACS Nano* **2018**, *12*, 5003-5010.

[29] B. Jiang, X. Zou, J. Su, J. Liang, J. Wang, H. Liu, L. Feng, C. Jiang, F. Wang, J. He, L. Liao, *Adv. Funct. Mater.* **2018**, *28*, 8.

[30] H. B. Michaelson, *J. Appl. Phys.* **1977**, *48*, 4729.

[31] [a)]S. D. Stranks, G. E. Eperon, G. Grancini, C. Menelaou, M. J. Alcocer, T. Leijtens, L. M. Herz, A. Petrozza, H. J. Snaith, *Science* **2013**, *342*, 341. [b)]G. E. Eperon, V. M. Burlakov, P. Docampo, A. Goriely, H. J. Snaith, *Adv. Funct. Mater.* **2014**, *24*, 151.

[32] [a)]G. Q. Tang, P. You, Q. D. Tai, R. S. Wu, F. Yan, *Solar RRL*, **2018**, *2*, 1800066. [b)]Z. K. Liu, P. You, C. Xie, G. Q. Tang, F. Yan, *Nano Energy*, **2016**, *28*, 151.

[33] Y. Akahama, M. Kobayashi, H. Kawamura, *Solid State Commun.* **1997**, *104*, 311.

[34] J.-R. Chen, P. M. Odenthal, A. G. Swartz, G. C. Floyd, H. Wen, K. Y. Luo, R. K. Kawakami, *Nano Lett.* **2013**, *13*, 3106.

[35] W. Wang, Y. Liu, L. Tang, Y. Jin, T. Zhao, F. Xiu, *Sci. Rep.* **2014**, *4*, 6928.

[36] C. Funck, A. Marchewka, C. Bäumer, P. C. Schmidt, P. Müller, R. Dittmann, M. Martin, R. Waser, S. Menzel, *Adv. Electron. Mater.* **2018**, *4*, 1800062.

[37] M. Farmanbar, G. Brocks, *Phys. Rev. B* **2015**, *91*, 161304.

[38] J. Wang, Q. Yao, C.-W. Huang, X. Zou, L. Liao, S. Chen, Z. Fan, K. Zhang, W. Wu, X. Xiao, C. Jiang, W.-W. Wu, *Adv. Mater.* **2016**, *28*, 8302.

[39] P. J. Jeon, Y. T. Lee, J. Y. Lim, J. S. Kim, D. K. Hwang, S. Im, *Nano Lett.* **2016**, *16*, 1293.

[40] D. Kufer, I. Nikitskiy, T. Lasanta, G. Navickaite, F. H. L. Koppens, G. Konstantatos, *Adv. Mater.* **2015**, *27*, 176.

[41] S. Teitsworth, R. Westervelt, *Phys. Rev. Lett.* **1984**, *53*, 2587.

[42] D. L. Shao, J. Gao, P. Chow, H. T. Sun, G. Q. Xin, P. Sharma, J. Lian, N. A. Koratkar, S. Sawyer, *Nano Lett.* **2015**, *15*, 3787.

[43] X. Liu, L. L. Gu, Q. P. Zhang, J. Y. Wu, Y. Z. Long, Z. Y. Fan, *Nat. Commun.* **2014**, *5*, 4007.

[44] Kim, C. O.; Kim, S.; Shin, D. H.; Kang, S. S.; Kim, J. M.; Jang, C. W.; Joo, S. S.; Lee, J. S.; Kim, J. H.; Choi, S.-H. *Nat. Commun.* **2014**, *5*, 3249.

[45] [a)]C. Xie, C. Mak, X. Tao, F. Yan, *Adv. Funct. Mater.* **2017**, *27*, 1603886. [b)]C. Xie and F. Yan, *Small*, **2017**, *20*, 1701822.

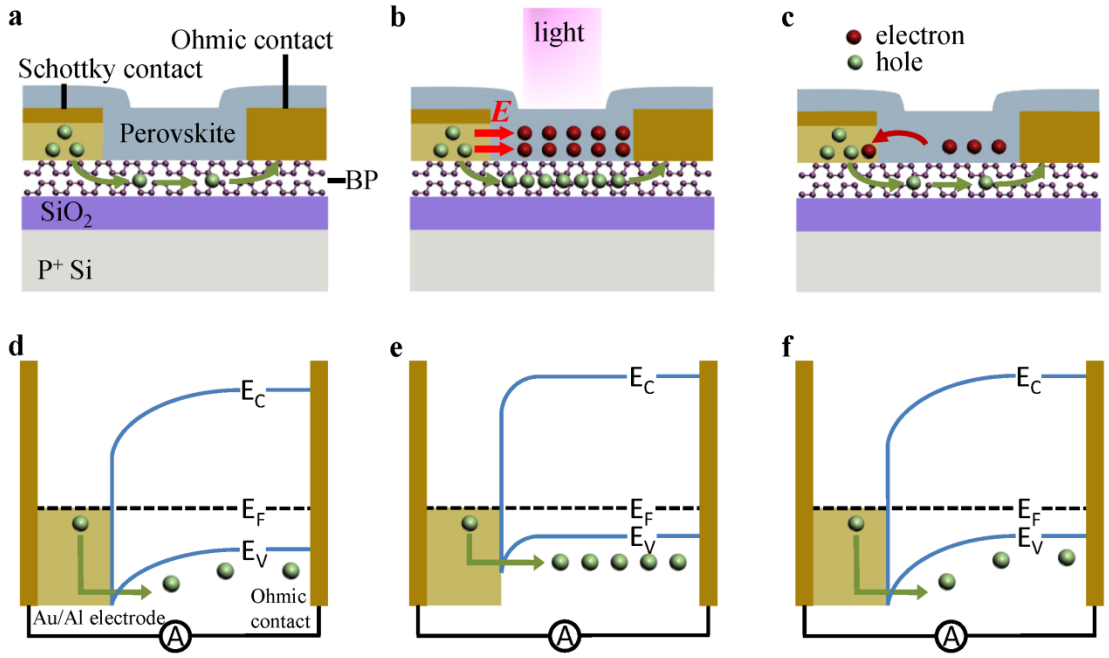

Figure 1. Illustration of the design concept and working principle. a) In the absence of illumination, the dark current is limited by the Schottky barrier at source electrode. b) Under illumination, photon-generated excitons will be separated into free holes in the BP and electrons in the perovskite. c) As the illumination is turned off, the trapped electrons will inject into the anode due to the strong local electric field *E* near the Schottky barrier. d-f) Schematic band diagrams of a metal/BP Schottky contact for the corresponding situations in **a-c**, respectively.

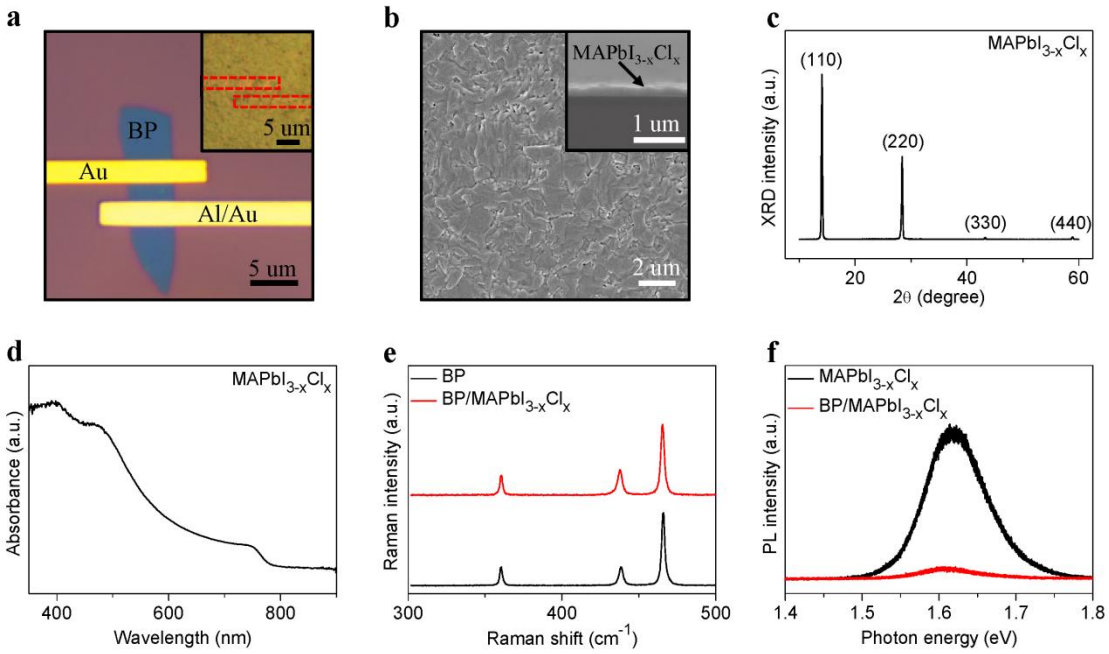

Figure 2. Characterization of BP/$MAPbI_{3-x}Cl_x$ hybrid films. a) Optical image of a typical BP/$MAPbI_{3-x}Cl_x$ Schottky FET. The inset shows the same device decorated with $MAPbI_{3-x}Cl_x$ perovskite. b) A typical plane view SEM image of the $MAPbI_{3-x}Cl_x$ perovskite on silicon substrate. The inset gives the corresponding cross-sectional SEM image. c) Absorption spectra of the $MAPbI_{3-x}Cl_x$ perovskite film on glass. d) XRD spectrum of $MAPbI_{3-x}Cl_x$ perovskite on silicon substrate. e) Raman spectra of the pristine BP and BP/$MAPbI_{3-x}Cl_x$ hybrid structure measured under 532 nm laser excitation. f) PL spectra measured for $MAPbI_{3-x}Cl_x$ perovskite and the BP/$MAPbI_{3-x}Cl_x$ hybrid structure.

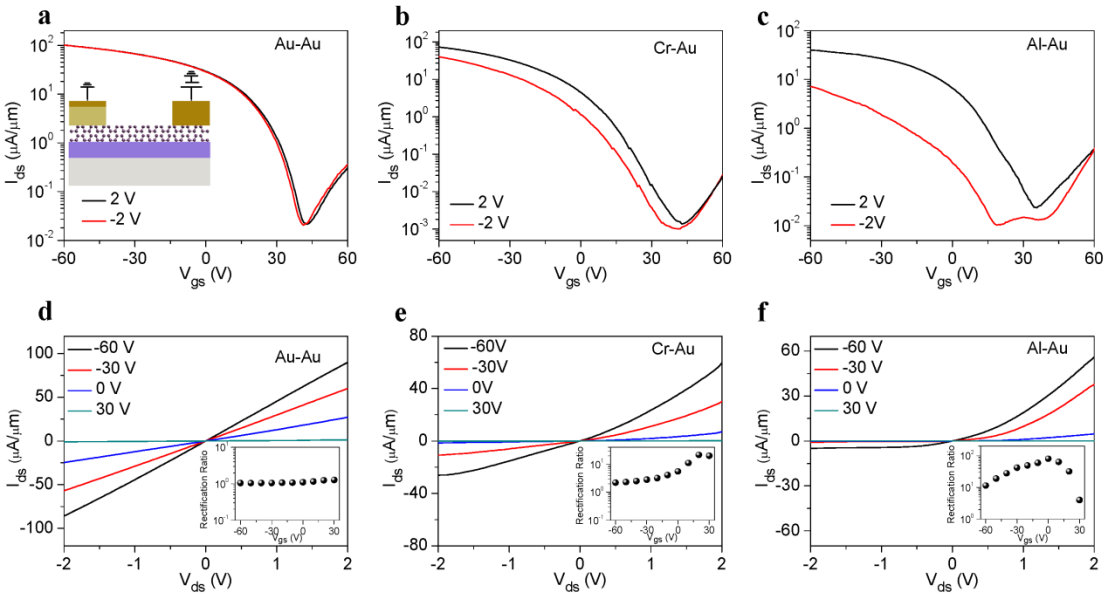

Figure 3. Electrical properties of back-gated BP FETs. a-c) Transfer characteristics (I_{ds}-V_{gs}) of the BP FETs for both forward and reverse V_{ds} bias with electrodes of Au-Au, Cr-Au and Al-Au, respectively. Au (60 nm) electrodes are deposited as the drain contact while Au (60nm), Cr/Au (60/20 nm) and Al/Au (60/20 nm) electrodes are deposited as the source contacts in three devices. d-f) Output characteristics (I_{ds}-V_{ds} at different gate voltage V_{gs}) of the devices with electrodes of Au-Au, Cr-Au and Al-Au, respectively. The insets show the rectification ratio.

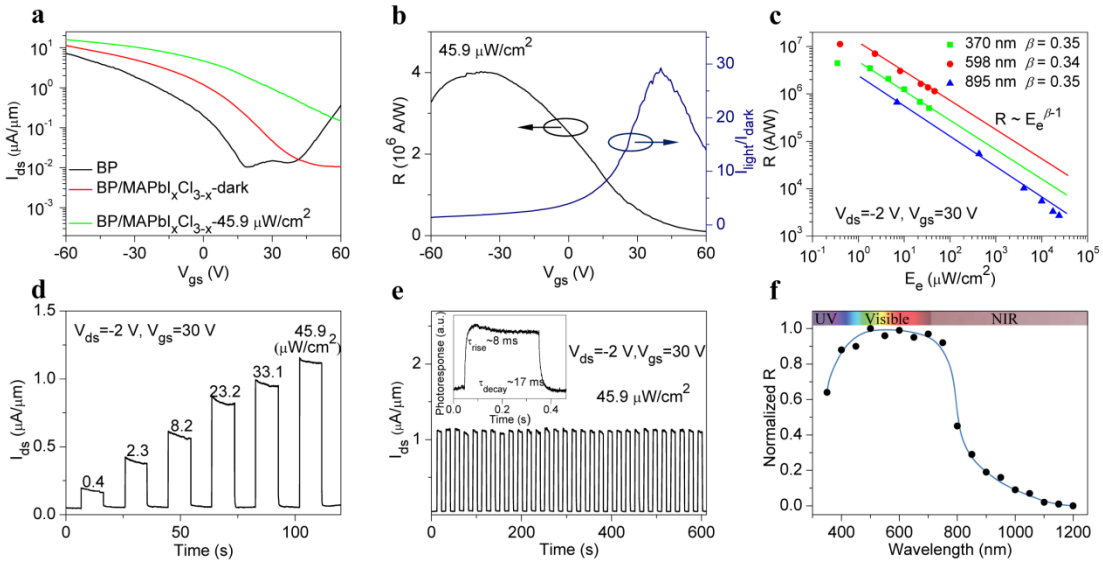

Figure 4. Optoelectronic characteristics of BP/$MAPbI_{3-x}Cl_x$ phototransistors with Al-Au electrodes operated under a reverse bias of -2 V. a) Transfer characteristics of the BP FET before and after $MAPbI_{3-x}Cl_x$ perovskite deposition. The transfer characteristic of the BP/$MAPbI_{3-x}Cl_x$ phototransistor under 598 nm light illumination is also presented. b) Responsivity and I_{light}/I_{dark} values of the same device as a function of applied gate voltage. c) Responsivity of the device under different illumination levels (λ: 370, 598, and 895 nm). d) Current under different light intensities of the same device operated under a backside gate voltage of 30 V. e) Dynamic response of the BP/$MAPbI_{3-x}Cl_x$ phototransistor measured in thirty period of modulation of the light intensity (λ = 598 nm, E_e = 45.9 μW/cm^2). The inset is rise (decay) time of the device recorded by an oscilloscope. We can estimate a rise (decay) time of 8 ms (17 ms). f) Normalized spectral responsivity of a device (wavelengths: from 350 to 1200 nm).

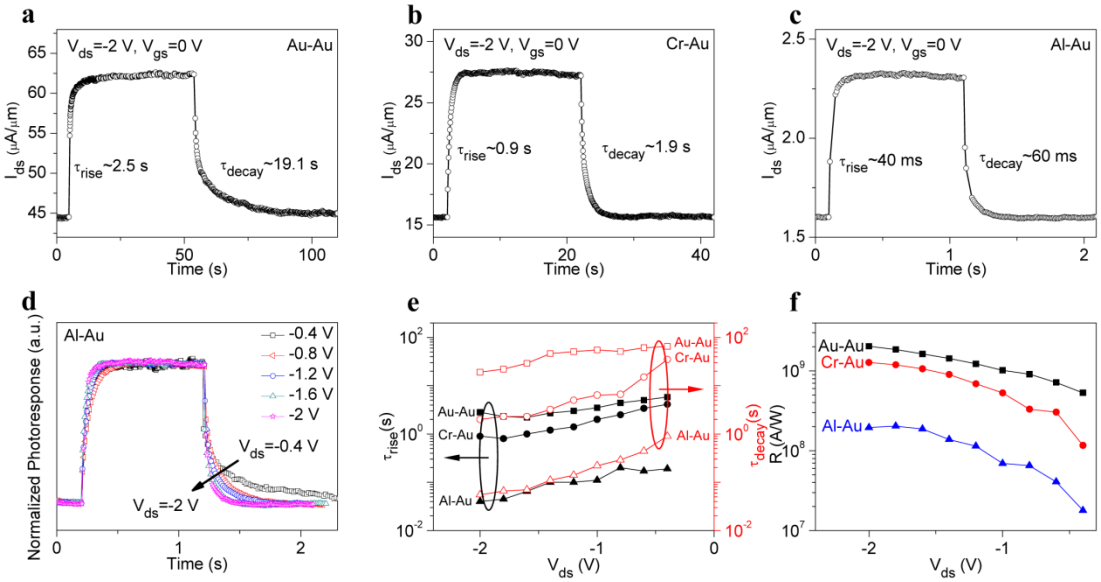

Figure 5. Dynamic response of BP/$MAPbI_{3-x}Cl_x$ phototransistors. a-c) Time-resolved photoresponse of the hybrid phototransistors with different electrodes (Au-Au, Cr-Au and Al-Au) measured at V_{ds} = -2 V and V_{gs} = 0 V (E_e = 0.4μW/cm^2). d) Time-resolved photoresponse of the Al-Au Schottky phototransistor as a function of reverse bias. e) Drain voltage dependence of the rise time and decay time. f) Drain voltage dependence of the responsivity.

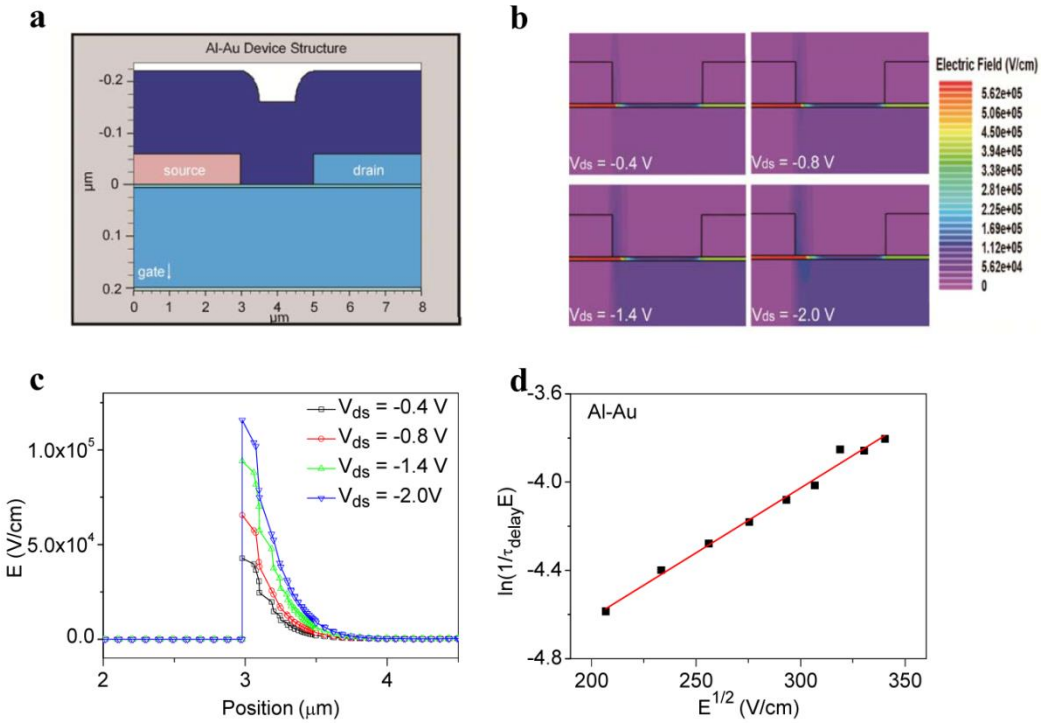

Figure 6. Device simulations of BP/Perovskite phototransistors. a) The structure of the simulated BP/$MAPbI_{3-x}Cl_x$ phototransistor with Al-Au electrode. b) Simulated electric field contour plot for the BP/$MAPbI_{3-x}Cl_x$ phototransistor. c) The extracted electric field close to the source electrode under different V_{ds}. d) The FP plot of $ln(1/\tau_{decay}E)$ *vs* $sqrt(|E|)$, which yields a straight line and is a proof for the validity of FP emission model.

The table of contents entry

High responsive photodetection of two-dimensional layered materials can be achieved by employing photogating mechanism. However, the corresponding response time is rather slow. Here, a Schottky barrier-controlled phototransistor is reported. A fast response is obtained via a field-assisted detrapping process of electrons in the perovskite layer. This provides a feasibility to achieve high-performance photodetector with both high responsivity and fast response.

Key words: phototransistor; black Phosphorus; perovskite; ultrahigh sensitivity; fast response

*Xuming Zou, Yuanzhe Li, Guanqi Tang, Peng You, and Feng Yan**

Schottky Barrier-Controlled Black Phosphorus/Perovskite Phototransistors with Ultrahigh Sensitivity and Fast Response